

Capillary pressure contribution in fabrics as a function of fibre volume fraction for Liquid Composite Moulding processes

H.N. Vo, Monica Francesca Pucci, S. Drapier, Pierre-Jacques Liotier

▶ **To cite this version:**

H.N. Vo, Monica Francesca Pucci, S. Drapier, Pierre-Jacques Liotier. Capillary pressure contribution in fabrics as a function of fibre volume fraction for Liquid Composite Moulding processes. Colloids and Surfaces A: Physicochemical and Engineering Aspects, 2022, 635, pp.128120. 10.1016/j.colsurfa.2021.128120 . hal-03518822

HAL Id: hal-03518822

https://imt-mines-ales.hal.science/hal-03518822

Submitted on 7 Jun 2022

HAL is a multi-disciplinary open access archive for the deposit and dissemination of scientific research documents, whether they are published or not. The documents may come from teaching and research institutions in France or abroad, or from public or private research centers.

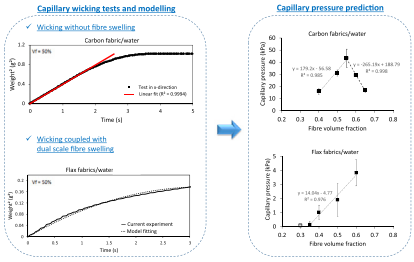
L'archive ouverte pluridisciplinaire **HAL**, est destinée au dépôt et à la diffusion de documents scientifiques de niveau recherche, publiés ou non, émanant des établissements d'enseignement et de recherche français ou étrangers, des laboratoires publics ou privés.

Capillary pressure contribution in fabrics as a function of fibre volume fraction for Liquid Composite Moulding processes

H.N. Vo [a,b], M.F. Pucci [c,*], S. Drapier [a], P.J. Liotier [d]

[a] Mines Saint-Etienne, Université de Lyon, CNRS, UMR 5307 LGF, Centre SMS, 158 Cours Fauriel, 42023 Saint-Etienne, France
[b] Department of Chemistry, College of Natural Sciences, Can Tho University, Campus II, 3/2 Street, Nink Kieu District, Can Tho City, Viet Nam
[c] LMGC, IMT Mines Ales, Université de Montpellier, CNRS, 6 Avenue de Clavières, 30100 Ales, France
[d] Polymers Composites and Hybrids (PCH), IMT Mines Ales, 6 Avenue de Clavières, 30100 Ales, France

GRAPHICAL ABSTRACT



ARTICLE INFO

Keywords:
Capillary pressure
Permeability
LCM processes

ABSTRACT

Liquid Composite Moulding processes are considered as promising and effective to manufacture structure composite parts reinforced with synthetic and natural fabrics. The main novelty of this work is the estimation of capillary pressure (P_{cap}) for both fabrics at different fibre volume fractions (V_f) and with different liquids. From the previous works, the P_{cap} was defined as the equivalence between Washburn's equation and Darcy's law while our novel model for the capillary wicking could predict very well the swelling behaviour of natural fabrics. The combination of our P_{cap} definition and our novel model was explored in this study. Linear trends, thresholds and extremums of P_{cap} at different conditions were found for the first time. These results are relevant to estimate the importance of capillary effects during Liquid Composite Moulding processes and extremely valuable for nu-merical models at the fibrous scale to predict voids formation.

1. Introduction

The need of manufacturing large composite parts in the transportation industry is driving the extension of Liquid Composite Moulding (LCM) processes. Those processes are known as efficient and cost effective but some issues about impregnation in fabrics remain and can induce voids or dry spots [1–3]. On the other hand, natural fibres have interesting properties, low density and better sustainability [4–8]. Composites reinforced by flax fibres have been shown to exhibit in some cases a specific modulus comparable or even higher than that of glass fibre reinforced composites [9]. However, it appears that the impregnation issues could be more significant with natural fibres due to their

* Corresponding author.
E-mail address: monica.pucci@mines-ales.fr (M.F. Pucci).

surface properties [10–12].

During the impregnation of resin in the fibre network, there is a competition between viscous and capillary effects that are related to the dimensionless capillary number *Ca* [13–17]. Different type of defects at different localisation can occur during manufacturing depending on the *Ca*. Some experimental and numerical studies were carried out to investigate voids entrapment and its dependence on the *Ca*. These studies, mostly in Resin Transfer Moulding, aim to determine optimal process parameters, controlling velocity during impregnation in fabrics [18–20].

In the LCM processes, the impregnation in fabric by resin is commonly driven by a pressure gradient. Resin Transfer Moulding (RTM) utilises positive operating pressures. However, such injection pressure is commonly low because high pressure can cause fibre misalignment and fibre breakage [21]. In Vacuum Infusion (VI), the pressure is lower than the atmospheric pressure and is limited to − 1 bar. In case of Vacuum Assisted Resin Transfer Moulding (VARTM), the system operates with positive injection pressure while the mould cavity is kept under vacuum [22]. In these processes, low pressure is used, meaning that all other forms of pressure such as capillary pressure (P_{cap}) cannot be neglected [23]. This is because such pressure can contribute to the overall pressure gradient to drive flow front movement. Hence, an error in calculation of the overall pressure gradient can occur if the capillary pressure is not considered [23,24]. In numerical models, the pressure gradient has been modified introducing a pressure drop at the flow front [25–27]. Experimentally, different authors in literature have proposed some methods to estimate P_{cap} [21,23,28–33].

P_{cap} is a homogenised representation of local wetting effects that depends on the morphology of the medium and its interaction with the liquid. The P_{cap} was fundamentally estimated using the Young-Laplace's equation [34]. In this case, some shape factors appear to take into account the flow direction, depending on the geometrical configuration of fabrics. The Young-Laplace's equation was used coupled with the Darcy's law, measuring simultaneously the P_{cap} with the permeability [21, 31,32]. A similar definition of P_{cap} and the permeability test were proposed by Verrey et al., 2005 [30], where a parameter representing the area of fibre-matrix interface per unit volume of matrix appears. It allows the authors to estimate the P_{cap} under a constant applied pressure gradient and at a constant flow rate. Shape factors are difficult to measure, and results depend on such parameters. Using the same permeability test of Verrey et al., 2005, Francucci et al., 2012 [35] found that the P_{cap} increased with higher fibre volume fraction (V_f) and capillary effects and micro flows are more dominant in natural fabrics than synthetic fabrics.

Other works focused on the spontaneous capillary wicking and the regime of wetting to determine the P_{cap} [23,36,37]. For example, an experiment was designed by Batch et al., 1996 [36] to measure capillary flow by the rate of weight gain of fibre-filled tube. The driving force for this flow was only P_{cap} and no external driving pressure was applied during impregnation. In the same line with this concept, the previous study of the authors introduced a new definition of P_{cap}, also using the capillary wicking test in fibre-filled hollow cylinder [33]. This definition takes an equivalence between Washburn's equation and Darcy's law. The P_{cap} thus depends on parameters accounting for the geometry of the porous medium, the fluid-solid interactions and the medium permeability. The geometrical parameters and the fluid-solid interactions were experimentally determined by capillary wicking test while the magnitude of permeability was chosen. As a result, the estimated values of P_{cap} were close to the ones found in literature [21,30] and these values have been introduced to finite element simulations to describe more accurately LCM processes for composite parts [25].

Most of studies in the P_{cap} focus on synthetic fabrics (carbon, glass) which the geometrical configuration does not change during the impregnation. On the other hand, very few studies on the P_{cap} with natural fabrics have been found in the literature [38]. This is mostly because natural fibres have not a stable morphology during wicking as observed in the previous studies of the authors [39,40]. However, it is interesting to mention that our novel model developed in the previous works [39,40] can predict very well the capillary wicking in flax fabrics at different V_f, taking into account the multi-scale swelling effects of the fibres at the elementary fibre level and at the individual yarn level.

The ambition of the present work is thus to estimate the P_{cap} in carbon fabrics and for the first time in flax fabrics. This work is the combination of our definition about P_{cap} with our novel model predicting capillary wicking in natural fabrics. The main novelty of this approach resides in two aspects: the study of P_{cap} in natural fabrics with a Washburn advancing contact angle estimated for a model from the previous works [39,40] and the correlation between the P_{cap} and the V_f, for both types of fabrics (carbon vs flax) and of liquids (n-hexane vs water).

2. Theory

2.1. Equivalence law for capillary pressure (P_{cap})

Assuming that fibre bundles inserted into a hollow cylinder can be regarded as a pack of capillary tubes [33] and according to the conventional Washburn's equation, the linear evolution of squared mass gain as a function of time should be obtained in constant porous medium. This can be expressed as follows neglecting gravity effects [41]:

$$m^2(t) = \left[\frac{(c\bar{r})\varepsilon^2(\pi R^2)^2}{2}\right]\frac{\rho^2\gamma_L cos\theta_a}{\eta}t \tag{1}$$

where c is a parameter taking into account tortuosity, $\bar{r}$ is the mean porous radius, ε is the porosity, which is considered as $1 - V_f$ (V_f: the fibre volume fraction), and R is the radius of a hollow cylinder. ρ, γ_L *and* η are the liquid density, surface tension and viscosity, respectively and θ_a is the apparent equivalent advancing contact angle. For constant medium porosity (related to geometric product $c\bar{r}$), Eq. (1) fits very accurately to the experimental data for synthetic fabrics over time [33,40].

The flow of liquid in a porous medium can also be described by the Darcy's law [42]. This equation relates an equivalent fluid velocity ν_D to a pressure drop with the help of permeability K, characterizing the ability of a porous medium to be crossed by a liquid of viscosity η:

$$\nu_D = -\frac{K}{\eta}\frac{dP}{dh} \tag{2}$$

In the case of wicking of fibre bundles into a hollow cylinder, Eq. (2) was rewritten considering the porosity ε and introducing a negative P_{cap} in the pressure gradient. Integrating linearly the Darcy's law and rewriting this expression as a function of the squared mass gain, a linear relation over time was obtained [33]:

$$m^2(t) = \frac{2K\varepsilon\rho^2(\pi R^2)^2 P_{cap}}{\eta}t \tag{3}$$

where R is the radius of the cylindrical sample holder and ρ is the liquid density.

In order to give a physical meaning to the P_{cap}, it is thus possible to state the equivalence between the Washburn (Eq. (1)) and the Darcy (Eq. (3)) equations describing the wicking of porous medium. The resulting

expression is:

$$P_{cap} = (c\bar{r})\varepsilon\frac{\gamma_L cos\theta_a}{4K} \quad (4)$$

The P_{cap} thus depends both on the porous medium morphology (a parameter related to tortuosity c, mean capillary radius $\bar{r}$, porosity ε and the medium permeability K) and parameters taking into account the interactions between the fluid and the porous medium (surface tension of the fluid γ_L and the apparent advancing contact angle θ_a).

2.2. The interpretation of capillary pressure calculation

In this work, the P_{cap} values of carbon and flax fabrics are calculated using Eq. (4). The porosity ε is considered as $1 - V_f$ and the surface tension of the fluid γ_L is taken from Table 1 (Section 3.2). This means that the medium permeability K, the geometric product $c\bar{r}$ and the apparent advancing contact angle θ_a need to be determined in order to determine P_{cap}.

Based on regularly ordered and aligned filaments, equation of permeability along the fibres $K_{//}$ was derived by Gebart [43]:

$$K_{//} = \frac{8R_f^2}{\varsigma}\frac{(1-V_f)^3}{V_f^2} \quad (5)$$

where R_f is the fibre radius (3.5 μm for carbon fibre and 10 μm for flax fibre are the mean values that are considered in this study) and ς is the shape factor with the value of 53 for a hexagonal arrangement [43].

The geometric product $c\bar{r}$ and the apparent advancing contact angle θ_a are determined by capillary wicking test using Eq. (1). In the constant porous medium, e.g. carbon fabrics, the evolution of squared mass gain as a function of time was linearly observed with both n-hexane and water as described in conventional Washburn's equation. The geometric product $c\bar{r}$ is first determined with n-hexane. Such liquid is considered as a totally wetting liquid which has an apparent equivalent advancing contact angle of 0°. Once $c\bar{r}$ is known, it can be substituted into Eq. (1) again. Hence, the apparent advancing contact angle θ_a can be calculated through a wicking test with water.

2.3. Adaptation to dual scale swelling of natural fibres

However, for natural fibres, the porous medium changes over time during wicking of water, due to fibre swelling. In this case, the wicking test with n-hexane can only be used to determine the initial non-swollen geometrical parameter of the fibrous medium $(c\bar{r})$. In a previous study of the authors [40], Washburn's model was modified, taking into account the fibre swelling at two scales, i.e. elementary fibres and individual yarns. The $(c\bar{r})$ can now be expressed as a function of the surface ratio $(\varnothing_{yarn})$ of yarn in a section of a fabric made of natural fibres:

$$c\bar{r} = c\left(\left(1-\varnothing_{yarn}\right)\overline{R} + \varnothing_{yarn}\overline{r}'\right) \quad (6)$$

where $\overline{R}$ is the inter yarn mean pore radius and $\overline{r}'$ the intra yarn mean pore radius [40].

During swelling of fibres and the associated swelling of yarns, the mean pore radiuses decrease along with the swelling rate of both fibres and yarns. Those two parameters have been identified in authors previous work as linear [40]. Eqs. (7) and (8) can thus be written:

$$(c\bar{r})(t) = c\left(\left(1-\varnothing_{yarn}\right)(\overline{R}_0 - bt) + \varnothing_{yarn}\left(\overline{r}_0' - at\right)\right) \quad (7)$$

$$(c\bar{r})(t) = (c\bar{r})_{ini} - ct\left(\left(1-\varnothing_{yarn}\right)b + \varnothing_{yarn}a\right) \quad (8)$$

where $\overline{R}_0$ and $\overline{r}_0'$ are the initial pore radiuses, and a and b are the respective apparent swelling rates of fibres and yarns. Then it is possible to insert those assumption in the authors first model of wicking in reinforcements undergoing swelling [39] to be able to describe the deviation to Washburn's original law (Eq. (3)):

if $(c\bar{r})(t) > (c\bar{r})_{fin}$

$$(c\bar{r})(t) = (c\bar{r})_{ini} - ct\left(\left(1-\varnothing_{yarn}\right)b + \varnothing_{yarn}a\right) \quad (9)$$

else

$$(c\bar{r})(t) = (c\bar{r})_{fin} \quad (10)$$

The proposed model satisfactorily fits experimental results from capillary tests at different V_f, allowing to obtain the apparent advancing contact angles θ_a for flax fabrics with water. Fig. 1 shows a wicking test for the flax fabrics with water and the fit of this non-linear trend with model proposed in Vo et al. [40].

3. Experiments

3.1. Fabrics

Carbon and flax fabrics used in this study are quasi-unidirectional woven fabrics. Carbon fabrics were supplied by Hexcel with material code 48580®. Such fabrics contain 3% in volume of glass tows in weft direction. They have an areal weight of 541 g/m^2 and density of 1.8 g/m^3. Flax fabrics were provided by Libeco under the commercial designation FLAXDRY UD 180®. Their areal weight is 180 g/m^2 and density is 1.45 g/m^3. Both types of fabrics were used in our previous works dealing with wicking [33,39,40].

3.2. Test liquids

N-hexane and distilled water were selected in this study. The first one has low and totally dispersive surface tension, making it suitable for determination of the initial non-swollen geometrical parameters of the fibrous medium $(c\bar{r})$ appearing in the Washburn's equation (Eq. (1)). The second one was chosen to determine the apparent advancing contact angle θ_a from wicking tests. Contrarily to n-hexane, water is polar. With both liquids, P_{cap} is estimated for carbon and flax fabrics. Table 1 presents the surface tension, components, density and viscosity of these test liquids, as found in literature [44].

Table 1
Characteristic of test liquids at 20 °C.

	ρ (g/cm^3)	η (mPa s)	γ_L (mN/m)	γ_L^p (mN/m)	γ_L^d (mN/m)
N-hexane	0.659	0.32	18.4	0.0	18.4
Water	0.998	1.00	72.8	51.0	21.8

With ρ, η, γ_L, γ_L^p and γ_L^d representing respectively the density, viscosity, surface tension and its polar and dispersive components.

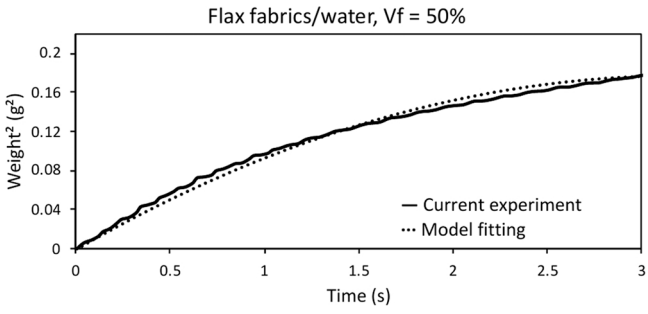


Fig. 1. Fitting of experimental wicking data with the model proposed in Vo et al. [40] at 50% V_f.

3.3. Wicking tests

The procedure was well described in details in previous works of the authors [33,40]. First, the amount of fabrics was calculated based on the total inner volume of the vertical sample holder consisting in a cylindrical tube (height of 20 mm and radius of 6 mm) [33] with certain V_f (V_f is considered as a ratio between the volume of fibre and the total inner volume of the cylindrical tube). The fabrics were then rolled along the transverse direction and inserted into a tube in order to study the wicking in the warp direction of fabric (parallel to fibre direction). The dynamic tests of capillary wicking were performed with a tensiometer (DCAT11, DataPhysics Instrument GmbH, Fildestrardt, Germany). The vertical tube was attached to the tensiometer and the base containing a vessel with a test liquid moved up towards the tube with a speed of 0.5 mm/s. The microbalance with weight detection of 10 μg was set. When the liquid touched the tube and the mass gain was higher than 10 μg, the base stopped moving and data of mass gain as a function of time started recording.

The wicking test was first performed with n-hexane. After weight saturation, the tube containing fibres was dried in an oven at 60 °C to let n-hexane evaporate. The mass loss was checked with microbalance until the weight did not change, the drying process took approximately two hours. The wicking test was then continued with water. All experiments were done at 20 °C and at least five individual tubes were tested for each fabric and with certain V_f. Fig. 2 shows an example of experimental data of the linear fits for carbon fabrics with n-hexane and with water. It is important to observe that the plateau achieved on figures is due to the liquid reaching the top of the sample and not due to an equilibrium induced by gravity effects.

Experiments in the present study were designed to investigate P_{cap} in fabrics in the warp direction varying the V_f. Wicking tests were performed in n-hexane and then in distilled water at different V_f (0.5, 0.55 and 0.65 for carbon fabrics, and 0.5 for flax fabrics). It should be noted that wicking at 40% V_f of carbon fabrics is repeated in this study in order to validate the proof of concept. Wicking tests for other V_f (0.3, 0.35, 0.4 and 0.6) were considered from the previous works [33,39,40].

4. Results and discussion

In order to calculate the value of P_{cap} for carbon and flax fabrics from Eq. (4), the medium permeability K, the geometric product $c\bar{r}$ and the advancing contact angle θ_a have to be determined for each V_f.

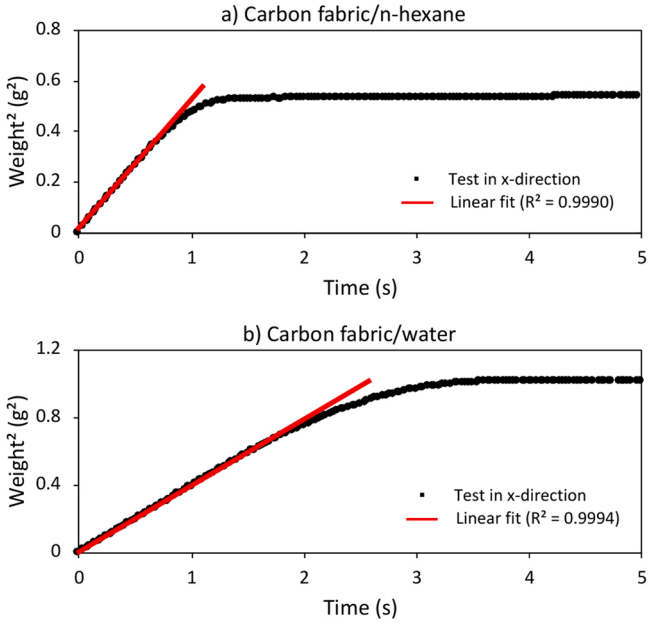


Fig. 2. Linear fit of a wicking test for carbon fabrics at 50% V_f with (a) n-hexane and (b) distilled water.

Table 2
Magnitude of permeability of carbon and flax fabrics with hexagonal packing at different V_f, according to Gebart [43].

V_f (%)	$K_{//}$ of carbon fabrics (μm²)	$K_{//}$ of flax fabrics (μm²)
30	7.0	57.5
35	4.1	33.8
40	2.5	20.4
50	0.9	7.5
55	0.6	4.5
60	0.3	2.7
65	0.2	1.5

4.1. Estimation of the medium permeability

An important parameter to determine the P_{cap} is the magnitude of permeability K. According to Gebart [43], this parameter depends on the fibre radius and fibre volume fraction, as shown in Eq. (5). Table 2 presents the value of permeability of carbon and flax fabrics at different V_f. K decreases as V_f increases and the magnitude of permeability of carbon fabrics is much lower than that of flax fabrics. This is logical because the radius of carbon fibre is much smaller than the one of flax fibre at the same V_f.

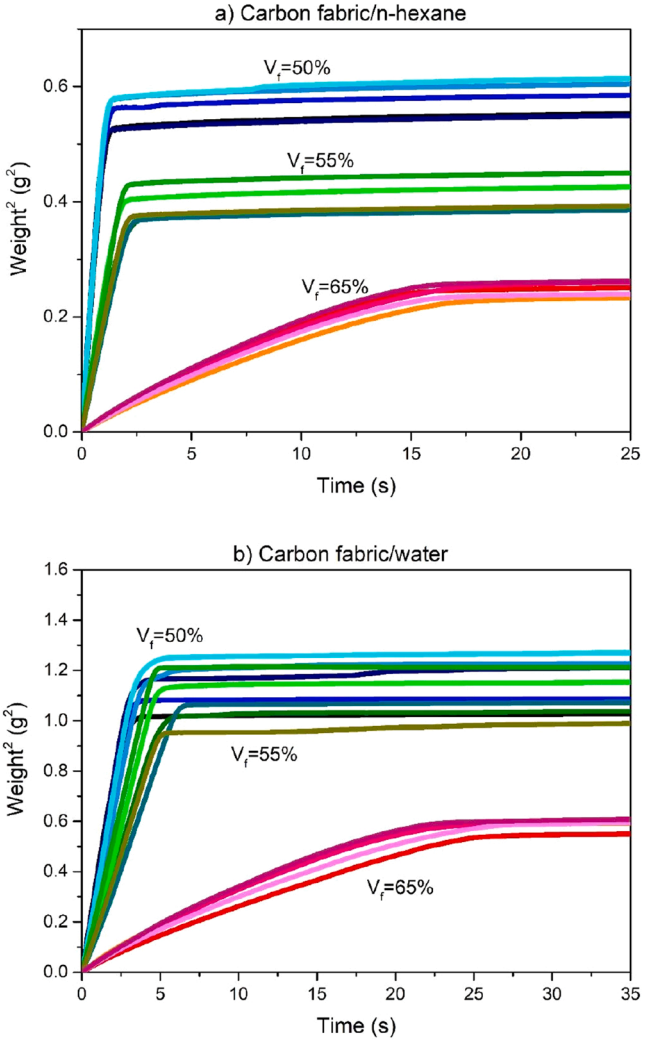


Fig. 3. Wicking curves in warp direction of carbon fabrics with (a) n-hexane and (b) distilled water at 50%, 55% and 65% V_f.

Table 3
Results of wicking tests for carbon fabrics with n-hexane at different V_f.

Carbon	$V_f = 50\%$			$V_f = 55\%$			$V_f = 65\%$		
	Linear slope	R^2	$c\bar{r}$ (μm)	*Linear slope*	R^2	$c\bar{r}$ (μm)	*Linear slope*	R^2	$c\bar{r}$ (μm)
Sample 1	0.504	0.999	12.6	0.196	0.998	6.1	0.018	0.996	0.9
Sample 2	0.555	0.999	13.9	0.236	0.999	7.3	0.016	0.996	0.8
Sample 3	0.514	0.999	12.9	0.177	0.999	5.5	0.018	0.995	0.9
Sample 4	0.523	0.998	13.1	0.231	0.999	7.1	0.017	0.996	0.9
Sample 5	0.538	0.999	13.5	0.190	0.999	5.9	0.019	0.995	1.0

4.2. Wicking in carbon fabrics

Following the procedure described in Section 3.3, the wicking tests were performed in the hollow tube for carbon fabrics with V_f of 50%, 55% and 65%. Fig. 3 shows the correlation between the squared mass gain and wicking time for carbon fabrics with different test liquids. The lowest V_f has the highest equilibrium mass because the high void space in between fibres can trap a higher amount of liquid at low fibre content. The linear trends of the wicking process for both liquids indicate that the conventional Washburn's equation (Eq. (1)) can be applied.

Tables 3 and 4 present the results of linear fitting with correlation coefficient (R^2) for each sample with n-hexane and water, respectively, and subsequently the determined geometric product $c\bar{r}$ and the advancing contact angle θ_a. The values of $c\bar{r}$ is lower at higher V_f. This is expected since $c\bar{r}$ is proportional to the void space in between the fibres which is lower at higher fibre content. According to Eq. (1), the apparent advancing contact angle θ_a is determined thanks to the geometric product $c\bar{r}$. Smaller θ_a commonly describes a faster capillary wicking but this can only be observed when the geometry is fixed [41]. Here, the geometry varies with the change of V_f and it is shown that, as seen for $c\bar{r}$, also the apparent advancing contact angle decreases as V_f increases.

4.3. Wicking in flax fabrics

The same wicking test and calculation method as for carbon fabrics were used for flax fabrics. Experiments were performed at V_f of 50%. Fig. 4 shows the results of wicking test for flax fabrics with squared mass gain as a function of time with n-hexane and then with distilled water. Initial linear curve with n-hexane indicates that Washburn's equation can be applied to determine the initial geometric product $c\bar{r}$, as shown in Table 5. In case of wicking with water, as expected, the linearity of wicking can no longer be observed. Swelling of flax fibres during wicking leads to an evolution of morphology of this porous medium (then of $c\bar{r}$) and hence Washburn's equation cannot be directly applied. Then, the model proposed in Vo et al. [40] including swelling of elementary flax fibres and yarns in water was used to fit wicking tests and determine the apparent advancing contact angle θ_a. Table 5 shows θ_a calculated from model for tested samples with water. The values of θ_a seem to fluctuate from one sample to another. However, considering the average value at this V_f (50%), the contact angle is decreasing at higher V_f, as observed in Table 6 (Section 4.4).

4.4. Summary on wicking parameters at different fibre volume fraction

The conventional Washburn's equation describes the linearity of squared mass gain as a function of time for invariant porous structure morphology. Hence the geometric product $c\bar{r}$ and the apparent advancing contact angle θ_a of carbon fabrics can be determined at each V_f. In the case of flax fabrics, the $c\bar{r}$ values were determined by following the Washburn's equation while the θ_a values were estimated by the model developed in the previous study of the author [40]. This model, which takes into account the swelling behaviour of natural fibres at different levels, can fit very well with different V_f. Table 6 shows the average wicking parameters for both carbon and flax fabrics obtained in this study and in the previous ones [33,39,40].

These results are coherent with the observation already mentioned: increasing the V_f, $c\bar{r}$ decreases and, even if the wicking kinetic is slower, the resulting advancing contact angle also decreases.

4.5. Determination of the equivalent capillary pressure

Now that the wicking parameters, i.e. the geometric product $c\bar{r}$ and the apparent advancing contact angle θ_a, and the permeability K have been determined, hence the P_{cap} can be calculated based on Eq. (4). Fig. 5 (and Table 7 for numerical values) shows the results of P_{cap} at different V_f for carbon and flax fabrics with both n-hexane and water. In

Table 4
Results of wicking tests for carbon fabrics with distilled water at different V_f.

Carbon	$V_f = 50\%$			$V_f = 55\%$			$V_f = 65\%$		
	Linear slope	R^2	θ_a (°)	*Linear slope*	R^2	θ_a (°)	*Linear slope*	R^2	θ_a (°)
Sample 1	0.383	0.999	74.8	0.207	0.999	68.7	0.024	0.996	63.5
Sample 2	0.382	0.999	76.3	0.244	0.999	69.1	0.029	0.992	49.8
Sample 3	0.359	0.999	76.1	0.176	0.999	69.9	0.030	0.994	55.2
Sample 4	0.316	0.999	78.0	0.268	0.999	66.4	0.027	0.993	57.5
Sample 5	0.360	0.999	76.7	0.195	0.999	69.3	0.031	0.993	56.3

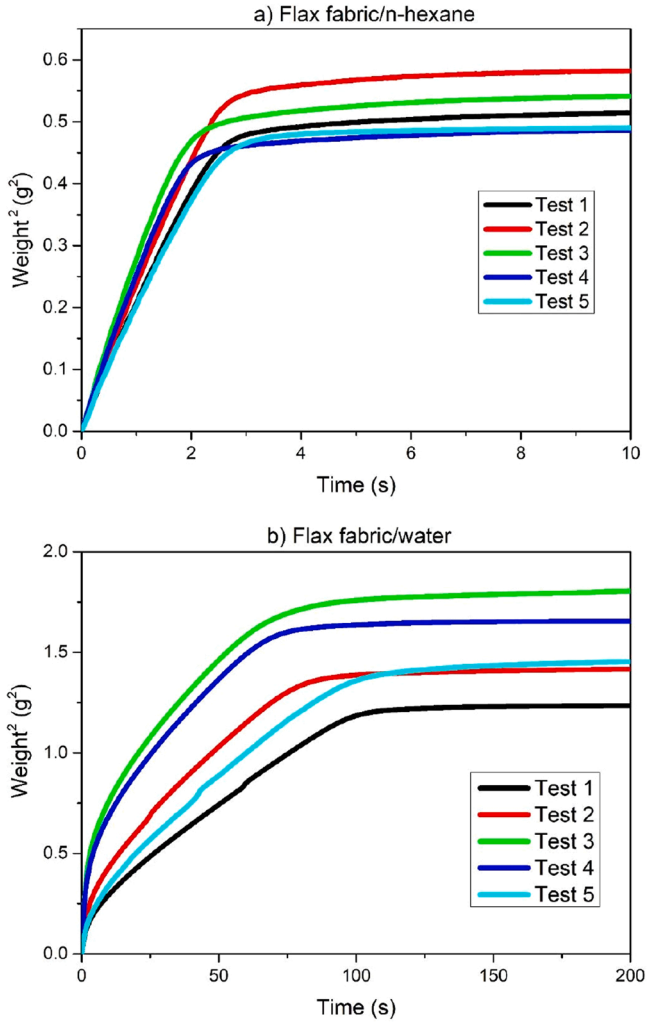


Fig. 4. Wicking curves in warp direction of flax fabrics with (a) n-hexane and (b) distilled water at 50% V_f.

case of carbon fabrics, it is interesting to note that there is a threshold at 55% V_f. The P_{cap} slightly decreases from 40% to 55% with n-hexane and then it drops significantly at 60% and 65%, corresponding to R^2 of 0.918 for this second part. On the other hand, when wicking with water, such pressure strongly increases from 40% to 55% V_f ($R^2 = 0.985$) and then decreases drastically with higher V_f ($R^2 = 0.998$). This has not been seen in literature and should be the focus of a further study.

Different behaviour was observed for wicking with flax fabrics. A linear increasing trend from low to high V_f was obtained for both n-hexane and water, corresponding to R^2 of 0.995 and 0.976, respectively. It should be noted that in case of water, P_{cap} at 30% V_f was not considered to take the linear trend because this value was almost zero, like at 35% V_f. This linear trend is in agreement with the study of Francucci et al., 2012 for the P_{cap} in jute fabrics with vinyl-ester [35]. Furthermore, the magnitude of P_{cap} for wicking in flax fabrics is much lower than in carbon fabrics. It is reasonable because the equation of P_{cap} (Eq. (4)) depends on the value of permeability K which is proportional to the fibre radius. Namely, flax fibre radius (around 10 μm for elementary fibre) is much higher than carbon fibre radius (around 3.5 μm). Hence P_{cap} in flax fabrics is much lower than in carbon fabrics, according to Gebart's permeability model [43].

Table 5
Results of wicking tests for flax fabrics with n-hexane at 50% V_f and the advancing contact angle θ_a with water estimated from model.

Flax	$V_f = 50\%$			
	Linear slope	R^2	$c\bar{r}$ (μm)	θ_a (°)[a]
Sample 1	0.197	0.999	4.9	81.5
Sample 2	0.223	0.998	5.6	77.5
Sample 3	0.268	0.998	6.7	65.0
Sample 4	0.244	0.998	6.1	67.5
Sample 5	0.194	0.998	4.9	81.0

[a] Data obtained through the previous model [40].

The magnitude of P_{cap} for wicking in carbon fabrics with n-hexane at 40% V_f is higher than that estimated by Pucci et al., 2015 [33] for the same unidirectional fibrous preforms. This difference lays on how the magnitude of permeability is obtained. Namely, the permeability in this paper is estimated using Gebart's equation with variation of V_f. On the other hand, the ones obtained in Pucci et al., 2015 were assumed based on the correlation between the three main directions, and these values were assumed constant in the first approach.

5. Conclusions

The presented work proposes a significant extension of methods previously published [25,39,40] confirming the large range of validity of the P_{cap} defined through wicking. The main novelty can be summarised in three principal conclusions.

The first one is that the P_{cap} depends on the tested liquid. It is the first time that the P_{cap} is also calculated for n-hexane. The second one is linked to the reliability of the model developed to consider the swelling of natural fibres. It was proved with the present results that the model is able to provide Washburn's equivalent advancing contact angles that can be used to calculate relevant P_{cap} with water in flax fabrics. The third and main novelty of this work resides in the study of the influence of V_f on P_{cap} for different liquids and fabrics. The principal conclusions

Table 6
Average wicking parameters of carbon and flax fabrics at different V_f.

Fabrics	V_f (%)	$c\bar{r}$ (μm)	θ_a (°)
Carbon	40	28.3 ± 2.4	82.7 ± 0.9
	50	13.0 ± 0.7	75.9 ± 1.5
	55	6.4 ± 0.8	68.7 ± 1.4
	60	2.3 ± 0.4(1)	55.4 ± 3.8(1)
	65	0.9 ± 0.1	56.5 ± 4.9
Flax	30	14.2 ± 0.8(2)	87.0 ± 0.3(3)
	35	13.4 ± 1.3(2)	76.5 ± 0.4(3)
	40	12.2 ± 1.4(2)	76.5 ± 1.0(3)
	50	5.7 ± 0.8	74.5 ± 7.7(3)
	60	3.8 ± 0.4(1)	68.3 ± 4.2(3)

(1) Data taken from Vo et al. [40].
(2) Data taken from Pucci et al. [39].
(3) Data obtained through the previous model [40].

obtained here are the linear trend of the P_{cap} as a function of V_f and that it can reach a maximum. Indeed, it was demonstrated that the P_{cap} could either be constant or vary linearly, depending on the type of fabrics (synthetic or natural) and liquids. A threshold value at which the trend is modified have been shown at 55% in carbon fabrics, while such a threshold could not be reached in flax fabrics. This might be due to the values of P_{cap} that are significantly lower in flax (ten times lowers).

The results obtained in the present study are of first interest for composite manufacturing simulation [25,26] and a major concern for complex part and 3D reinforcements [45]. Formulating an analytical description of the change of P_{cap} with V_f is thus the next step to be included in further numerical studies along with the understanding and predicting the occurrence of the threshold in further experimental studies.

Table 7
Capillary pressure in carbon and flax fabrics at different V_f.

Fabrics	V_f (%)	$P_{cap,\ n\text{-}hexane}$ (kPa)	$P_{cap,\ water}$ (kPa)
Carbon	40	31.3 ± 2.7	15.7 ± 2.6
	50	32.4 ± 1.6	31.1 ± 2.4
	55	30.0 ± 3.8	43.3 ± 7.4
	60	13.1 ± 2.0	29.0 ± 1.1
	65	7.7 ± 0.6	16.7 ± 1.6
Flax	30	0.4 ± 0.0	0.1 ± 0.1
	35	0.7 ± 0.1	0.1 ± 0.3
	40	1.1 ± 0.1	1.0 ± 0.5
	50	1.7 ± 0.2	1.9 ± 1.2
	60	2.6 ± 0.3	3.8 ± 0.9

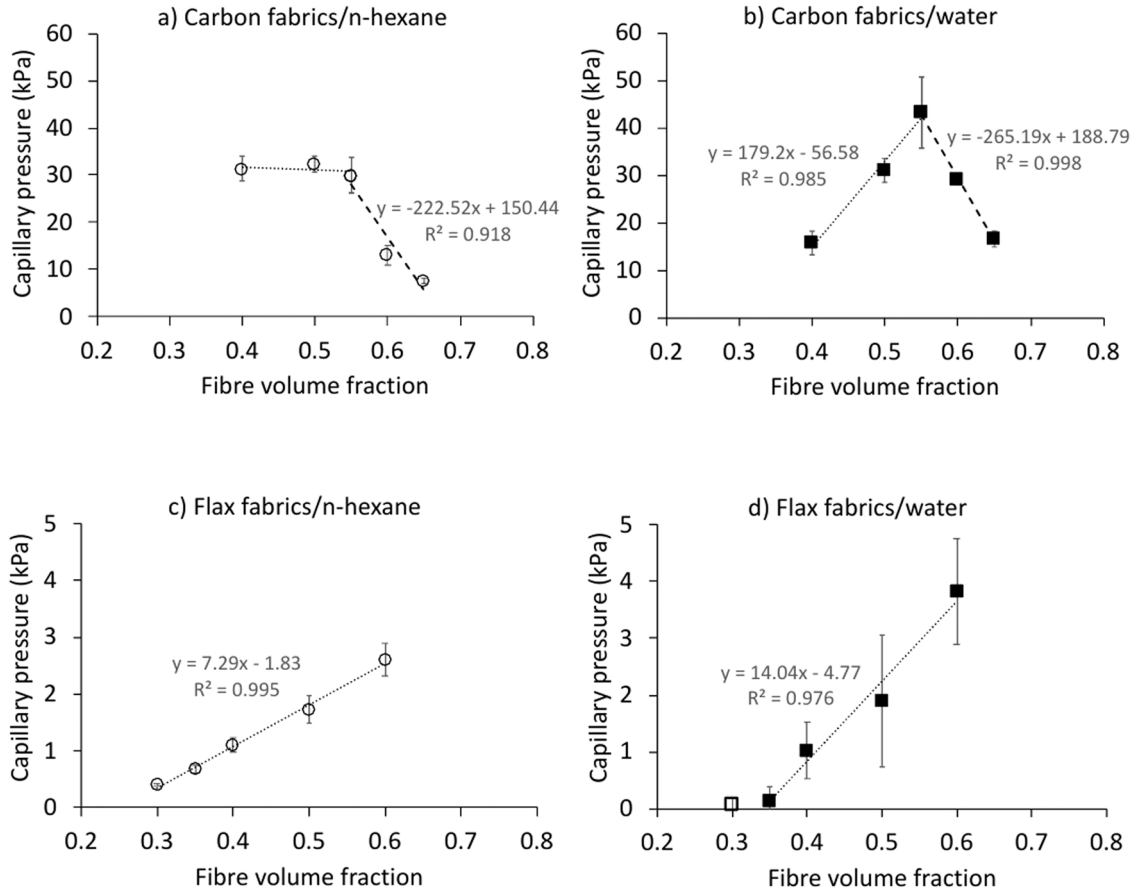


Fig. 5. Capillary pressure in carbon fabrics with n-hexane a) and water b); in flax fabrics with n-hexane c) and water d) at different V_f.

CRediT authorship contribution statement

H.N. Vo: Writing – original draft, Methodology, Investigation, Formal analysis. **M.F. Pucci:** Conceptualization, Validation, Methodology, Investigation, Formal analysis, Writing – review & editing. **S. Drapier:** Conceptualization, Methodology, Writing – review & editing. **P.J. Liotier:** Conceptualization, Validation, Methodology, Investigation, Supervision, Writing – review & editing.

Declaration of Competing Interest

The authors declare that they have no known competing financial interests or personal relationships that could have appeared to influence the work reported in this paper.

Data Availability

The raw data required to reproduce these findings cannot be shared at this time due to legal or ethical reasons.

References

[1] J. Bréard, A. Saouab, G. Bouquet, Numerical simulation of void formation in LCM, Compos. Part A Appl. Sci. Manuf. 34 (2003) 517–523, https://doi.org/10.1016/S1359-835X(03)00055-1.

[2] R.S. Parnas, A.J. Salem, T.A.K. Sadiq, H.-P. Wang, S.G. Advani, The interaction between micro- and macro-scopic flow in RTM preforms, Compos. Struct. 27 (1994) 93–107, https://doi.org/10.1016/0263-8223(94)90071-X.

[3] Z. Yousaf, P.J. Withers, P. Potluri, Compaction, nesting and image based permeability analysis of multi-layer dry preforms by computed tomography (CT), Compos. Struct. 263 (2021), 113676, https://doi.org/10.1016/j.compstruct.2021.113676.

[4] C. Baley, Analysis of the flax fibres tensile behaviour and analysis of the tensile stiffness increase, Compos. - Part A Appl. Sci. Manuf. 33 (2002) 939–948, https://doi.org/10.1016/S1359-835X(02)00040-4.

[5] A. Le Duigou, P. Davies, C. Baley, Environmental impact analysis of the production of flax fibres to be used as composite material reinforcement, J. Biobased Mater. Bioenergy 5 (2011) 153–165, https://doi.org/10.1166/jbmb.2011.1116.

[6] L.Q.N. Tran, C.A. Fuentes, C. Dupont-Gillain, A.W. Van Vuure, I. Verpoest, Wetting analysis and surface characterisation of coir fibres used as reinforcement for composites, Colloids Surf. A Physicochem. Eng. Asp. 377 (2011) 251–260, https://doi.org/10.1016/j.colsurfa.2011.01.023.

[7] C.A. Fuentes, L.Q.N. Tran, C. Dupont-Gillain, W. Vanderlinden, S. De Feyter, A. W. Van Vuure, I. Verpoest, Wetting behaviour and surface properties of technical bamboo fibres, Colloids Surf. A Physicochem Eng. Asp. 380 (2011) 89–99, https://doi.org/10.1016/j.colsurfa.2011.02.032.

[8] V. Placet, F. Trivaudey, O. Cisse, V. Gucheret-Retel, M.L. Boubakar, Diameter dependence of the apparent tensile modulus of hemp fibres: a morphological, structural or ultrastructural effect? Compos. Part A Appl. Sci. Manuf. 43 (2012) 275–287, https://doi.org/10.1016/j.compositesa.2011.10.019.

[9] P. Wambua, J. Ivens, I. Verpoest, Natural fibres: can they replace glass in fibre reinforced plastics? Compos. Sci. Technol. 63 (2003) 1259–1264, https://doi.org/10.1016/S0266-3538(03)00096-4.

[10] M.F. Pucci, P.J. Liotier, S. Drapier, Capillary effects on flax fibers - modification and characterization of the wetting dynamics, Compos. Part A Appl. Sci. Manuf. 77 (2015) 257–265, https://doi.org/10.1016/j.compositesa.2015.03.010.

[11] M.F. Pucci, P.J. Liotier, D. Seveno, C. Fuentes, A. Van Vuure, S. Drapier, Wetting and swelling property modifications of elementary flax fibres and their effects on the Liquid Composite Molding process, Compos. Part A Appl. Sci. Manuf. 97 (2017) 31–40, https://doi.org/10.1016/j.compositesa.2017.02.028.

[12] P.-J. Liotier, M.F. Pucci, A. Le Duigou, A. Kervoelen, J. Tirilló, F. Sarasini, S. Drapier, Role of interface formation versus fibres properties in the mechanical behaviour of bio-based composites manufactured by Liquid Composite Molding processes, Compos. Part B Eng. 163 (2019) 86–95, https://doi.org/10.1016/j.compositesb.2018.10.103.

[13] P.-G. De Gennes, Wetting: statics and dynamics, Rev. Mod. Phys. 57 (1985) 827.

[14] M.F. Pucci, B. Duchemin, M. Gomina, J. Bréard, Temperature effect on dynamic wetting of cellulosic substrates by molten polymers for composite processing, Compos. Part A Appl. Sci. Manuf. 114 (2018) 307–315, https://doi.org/10.1016/j.compositesa.2018.08.031.

[15] M.F. Pucci, B. Duchemin, M. Gomina, J. Bréard, Dynamic wetting of molten polymers on cellulosic substrates: model prediction for total and partial wetting, Front. Mater. 7 (2020) 143.

[16] K. Yoshihara, Y. Kamei, A. Mizuno, H. Ohgaki, T. Hori, I. Ueno, Effect of wettability on viscous fluid impregnation in single-layer woven-fibre bundles driven by pressure difference, Compos. Part A Appl. Sci. Manuf. 138 (2020), 106049, https://doi.org/10.1016/j.compositesa.2020.106049.

[17] V. Rougier, J. Cellier, M. Gomina, J. Bréard, Slip transition in dynamic wetting for a generalized Navier boundary condition, J. Colloid Interface Sci. 583 (2021) 448–458, https://doi.org/10.1016/j.jcis.2020.09.015.

[18] P. Celle, S. Drapier, J.-M. Bergheau, Numerical modelling of liquid infusion into fibrous media undergoing compaction, Eur. J. Mech - A/Solids 27 (2008) 647–661, https://doi.org/10.1016/j.euromechsol.2007.11.002.

[19] J.M. Lawrence, V. Neacsu, S.G. Advani, Modeling the impact of capillary pressure and air entrapment on fiber tow saturation during resin infusion in LCM, Compos. Part A Appl. Sci. Manuf. 40 (2009) 1053–1064, https://doi.org/10.1016/j.compositesa.2009.04.013.

[20] Y. Liu, N. Moulin, J. Bruchon, P.-J. Liotier, S. Drapier, Towards void formation and permeability predictions in LCM processes: a computational bifluid–solid mechanics framework dealing with capillarity and wetting issues, Comptes Rendus Méc. 344 (2016) 236–250, https://doi.org/10.1016/j.crme.2016.02.004.

[21] K.J. Ahn, J.C. Seferis, J.C. Berg, Simultaneous measurements of permeability and capillary pressure of thermosetting matrices in woven fabric reinforcements, Polym. Compos. 12 (1991) 146–152, https://doi.org/10.1002/pc.750120303.

[22] J.-I. Kim, Y.-T. Hwang, K.-H. Choi, H.-J. Kim, H.-S. Kim, Prediction of the vacuum assisted resin transfer molding (VARTM) process considering the directional permeability of sheared woven fabric, Compos. Struct. 211 (2019) 236–243, https://doi.org/10.1016/j.compstruct.2018.12.043.

[23] B. Willenbacher, D. May, P. Mitschang, Out–of–plane capillary pressure of technical textiles, Compos. Part A Appl. Sci. Manuf. 124 (2019), 105495, https://doi.org/10.1016/j.compositesa.2019.105495.

[24] S.G. Abaimov, O.V. Lebedev, V. Grishaev, B.N. Gilmutdinov, I.S. Akhatov, Edge flow profile under radial injection at constant pressure: analytical predictions vs. experiment, Compos. Struct. 242 (2020), 112101, https://doi.org/10.1016/j.compstruct.2020.112101.

[25] K. Andriamananjara, N. Moulin, J. Bruchon, P.-J. Liotier, S. Drapier, Numerical modeling of local capillary effects in porous media as a pressure discontinuity acting on the interface of a transient bi-fluid flow, Int. J. Mater. Form. 12 (2019) 675–691, https://doi.org/10.1007/s12289-018-1442-3.

[26] L. Chevalier, J. Bruchon, N. Moulin, P.J. Liotier, S. Drapier, Accounting for local capillary effects in two-phase flows with relaxed surface tension formulation in enriched finite elements, Comptes Rendus - Mec. 346 (2018) 617–633, https://doi.org/10.1016/j.crme.2018.06.008.

[27] M. Blais, N. Moulin, P.J. Liotier, S. Drapier, Resin infusion-based processes simulation: coupled Stokes-Darcy flows in orthotropic preforms undergoing finite strain, Int. J. Mater. Form. 10 (2017) 43–54, https://doi.org/10.1007/s12289-015-1259-2.

[28] V. Neacsu, A. Abu Obaid, S.G. Advani, Spontaneous radial capillary impregnation across a bank of aligned micro-cylinders – Part I: theory and model development, Int. J. Multiph. Flow 32 (2006) 661–676, https://doi.org/10.1016/j.ijmultiphaseflow.2006.02.006.

[29] V. Neacsu, A.A. Obaid, S.G. Advani, Spontaneous radial capillary impregnation across a bank of aligned micro-cylinders. Part II: experimental investigations, Int. J. Multiph. Flow 32 (2006) 677–691, https://doi.org/10.1016/j.ijmultiphaseflow.2006.02.015.

[30] J. Verrey, V. Michaud, J.A.E. Månson, Dynamic capillary effects in liquid composite moulding with non-crimp fabrics, Compos. Part A Appl. Sci. Manuf. 37 (2006) 92–102, https://doi.org/10.1016/j.compositesa.2005.04.011.

[31] V. Michaud, A. Mortensen, On measuring wettability in infiltration processing, Scr. Mater. 56 (2007) 859–862, https://doi.org/10.1016/j.scriptamat.2007.02.002.

[32] M. Nordlund, V. Michaud, Dynamic saturation curve measurement for resin flow in glass fibre reinforcement, Compos. Part A Appl. Sci. Manuf. 43 (2012) 333–343, https://doi.org/10.1016/j.compositesa.2011.12.001.

[33] M.F. Pucci, P.J. Liotier, S. Drapier, Capillary wicking in a fibrous reinforcement - orthotropic issues to determine the capillary pressure components, Compos. Part A Appl. Sci. Manuf. 77 (2015) 133–141, https://doi.org/10.1016/j.compositesa.2015.05.031.

[34] S. Amico, C. Lekakou, An experimental study of the permeability and capillary pressure in resin-transfer moulding, Compos. Sci. Technol. 61 (2001) 1945–1959, https://doi.org/10.1016/S0266-3538(01)00104-X.

[35] G. Francucci, A. Vázquez, E. Ruiz, E.S. Rodríguez, Capillary effects in vacuum-assisted resin transfer molding with natural fibers, Polym. Compos. 33 (2012) 1593–1602, https://doi.org/10.1002/pc.22290.

[36] G.L. Batch, Y.-T. Chen, C.W. Macoskot, Capillary impregnation of aligned fibrous beds: experiments and model, J. Reinf. Plast. Compos. 15 (1996) 1027–1051, https://doi.org/10.1177/073168449601501004.

[37] C. Ravey, E. Ruiz, F. Trochu, Determination of the optimal impregnation velocity in Resin Transfer Molding by capillary rise experiments and infrared thermography, Compos. Sci. Technol. 99 (2014) 96–102, https://doi.org/10.1016/j.compscitech.2014.05.019.

[38] R. Masoodi, K.M. Pillai, Darcy's law-based model for wicking in paper-like swelling porous media, AIChE J. 56 (2010) 2257–2267, https://doi.org/10.1002/aic.12163.

[39] M.F. Pucci, P.J. Liotier, S. Drapier, Capillary wicking in flax fabrics - effects of swelling in water, Colloids Surf. A Physicochem. Eng. Asp. 498 (2016) 176–184, https://doi.org/10.1016/j.colsurfa.2016.03.050.

[40] H.N. Vo, M.F. Pucci, S. Corn, N. Le Moigne, W. Garat, S. Drapier, et al., Capillary wicking in bio-based reinforcements undergoing swelling – dual scale consideration of porous medium, Compos. Part A Appl. Sci. Manuf. (2020) 134, https://doi.org/10.1016/j.compositesa.2020.105893.

[41] E.W. Washburn, Note on a method of determining the distribution of pore sizes in a porous material, Proc. Natl. Acad. Sci. USA (1921) 115–116, https://https://dx.doi.org/10.1073%2Fpnas.7.4.115.

[42] Darcy H. Les fontaines publiques de la ville de Dijon: exposition et application des principes à suivre et des formules à employer dans les questions de distribution d'eau. Victor Dalmont, 1856.
[43] B.R. Gebart, Permeability of unidirectional reinforcements for RTM, J. Compos. Mater. 26 (1992) 1100–1133, https://doi.org/10.1177/002199839202600802.
[44] C. Rulison, Wettability studies for porous solids including powders and fibrous materials, Appl. Note (1996) 302.
[45] A. Geoffre, Y. Wielhorski, N. Moulin, J. Bruchon, S. Drapier, P.-J. Liotier, Influence of intra-yarn flows on whole 3D woven fabric numerical permeability: from Stokes to Stokes-Darcy simulations, Int. J. Multiph. Flow 129 (2020), 103349, https://doi.org/10.1016/j.ijmultiphaseflow.2020.103349.